[CANCER RESEARCH 62, 307–312, January 1, 2002]

Noninvasive Imaging of Tumor Redox Status and Its Modification by Tissue Glutathione Levels[1]

Periannan Kuppusamy,[2] Haiquan Li, Govindasamy Ilangovan, Arturo J. Cardounel, Jay L. Zweier, Kenichi Yamada, Murali C. Krishna, and James B. Mitchell

The EPR Center and Division of Cardiology, Department of Medicine, Johns Hopkins University, School of Medicine, Baltimore, Maryland 21224 [P. K., H. L., G. I., A. J. C., J. L. Z.], and Radiation Biology Branch, National Cancer Institute, NIH, Bethesda, Maryland 20892 [K. Y., M. C. K., J. B. M.]

ABSTRACT

Therapeutic regimens such as radiation or chemotherapy attempt to exploit the physiological differences between normal and malignant tissue. Tissue redox status and pO_2 are two factors that are hypothesized to be different in normal and malignant tissues. Methods that can detect subtle differences in the above physiological parameters would greatly aid in devising appropriate treatment strategies. We have previously used *in vivo* electron paramagnetic resonance (EPR) spectroscopy and imaging techniques and shown that tumor tissues are highly reducing and hypoxic compared with normal tissues (P. Kuppusamy *et al.*, Cancer Res., *58:* 1562–1568, 1998). The purpose of the present study was to obtain spatially resolved redox data from normal and tumor tissues of radiation-induced fibrosarcoma (RIF-1) tumor-bearing mice and to examine the role of intracellular glutathione (GSH) on the tissue redox status. Experiments were performed using low-frequency (1.3 GHz) *in vivo* EPR spectroscopy and imaging techniques with a nitroxide redox probe. L-buthionine-*S,R*-sulfoximine (BSO), an inhibitor of GSH synthesis, was used to deplete tissue GSH levels. The results show the existence of significant heterogeneity of redox status in the tumor tissue compared with normal tissue. The tumor tissues show at least 4-fold higher concentrations of GSH levels compared with normal tissues in the tumor-bearing mice. Also BSO treatment showed a differential depletion of GSH and reducing equivalents in the tumor tissue. Thus, it appears that there is significant heterogeneity of tumor redox status and that manipulation of the tumor redox status may be important in tumor growth and therapy.

INTRODUCTION

The redox environment (1) within the tumor cell is an important parameter that may determine the response of a tumor to certain chemotherapeutic agents, radiation, and bioreductive hypoxic cell cytotoxins (2–5). A variety of intracellular molecules may contribute to the overall redox status in tissues including GSH,[3] thioredoxins, NADPH, flavins, ascorbate, and others (1). Collectively, the reducing species may have an impact on how a particular tissue responds to oxidative stress induced by a particular drug or treatment modality, and, therefore, a noninvasive means of determining the redox status of a tissue should be a useful adjunct for clinical oncology.

Low-molecular-weight, stable nitroxide free radicals have been used as biophysical and biochemical probes in a variety of biological experiments (6–8), in which EPR spectroscopy is conveniently used for detection. The nitroxides exist in biological systems as a redox pair (Fig. 1), namely the nitroxide free radical form and the diamagnetic hydroxylamine, which is the one-electron reduction product of the nitroxide free radical (9–11). Prior studies indicated that nitroxides are reduced to the corresponding hydroxylamine in cellular incubations as well as *in vivo* and that the rate of nitroxide reduction is significantly enhanced under hypoxic conditions (12–16). Presumably, the nitroxide accepts cellular reducing equivalents that would have gone to the reduction of molecular oxygen. Hence, the pharmacology of nitroxides in an EPR experiment should report on differences that exist in tissues having different redox and oxygen status. Previously we have estimated the *in vivo* levels of the unreduced nitroxide from excised tumor and found it to be significantly lower in tumor as compared with bone marrow (17). We further performed noninvasive *in vivo* EPR spectroscopic measurements of nitroxide reduction profiles in RIF-1 tumor-bearing mice and reported that the tumor tissues were significantly hypoxic and highly reducing compared with the normal tissues (18). Thus, measurement and mapping of nitroxide reduction profiles in tumor and normal tissues *in vivo* should provide important physiological information on tissue redox and oxygen status.

Thiols such as intracellular GSH and protein thiols are key to maintaining the redox status of tissues. Chemically, nitroxides do not react with thiols. However, in microsomal preparations, thiol-containing biomolecules have been shown to play a significant role in the bioreduction of nitroxides (19). Because thiol/disulfide state generally reflects the redox status of the tissue, altering the concentration of the thiol or changing the ratio of redox pairs should have an impact on the clearance of the nitroxide and, thus, provide a means to study the importance of this class of compounds as a function of bioreduction. For example, depleting the GSH levels by using specific inhibitors of its synthesis such as BSO and monitoring the pharmacokinetics of redox-sensitive nitroxide probes in both normal as well as tumor tissue should delineate the role of thiols in modulating tissue redox status.

The purpose of this study was: (*a*) to develop a noninvasive method to measure and image tissue redox status; (*b*) to obtain redox images *in vivo* from normal and tumor tissues of RIF-1 tumor-bearing mice; and (*c*) to examine the role of intracellular GSH on the tissue redox status. Experiments were performed using low-frequency (1.3 GHz) *in vivo* EPR spectroscopy and imaging techniques with a nitroxide redox probe. The results show the existence of significant heterogeneity in the redox status of the tumor tissue, and that there is differential depletion of the reducing equivalents in the tumor compared with normal tissue in mice treated with inhibitors of GSH synthesis.

MATERIALS AND METHODS

Chemicals. The nitroxide probe 3-CP was purchased from Aldrich (Milwaukee, WI). Solutions of the nitroxide were freshly prepared at a stock concentration of 300 mM in saline. GSH (L-γ-glutamyl-L-cysteinyl-glycine) and BSO were purchased from Sigma Chemical Co.

Mice. Female C3H mice were supplied through the Frederick Cancer Research Center Animal Production, Frederick, MD. The animals were received at 6 weeks of age and housed five per cage in climate-controlled rooms and were allowed food and acidified water *ad libitum*. The animals were on average 50 days old at the time of experimentation and weighed 25 ± 3 g.

Received 9/5/01; accepted 11/1/01.

The costs of publication of this article were defrayed in part by the payment of page charges. This article must therefore be hereby marked *advertisement* in accordance with 18 U.S.C. Section 1734 solely to indicate this fact.

[1] Supported by National Cancer Institute (NIH) Grants CA 78886 and RR 12190.

[2] To whom requests for reprints should be addressed, at Johns Hopkins University, School of Medicine, 5501 Hopkins Bayview Circle, Baltimore, MD 21224. Phone: (410) 550-3229; Fax: (410) 550-2448; E-mail: kuppu@welch.jhu.edu.

[3] The abbreviations used are: GSH, glutathione; 3-CP, 3-carbamoyl-2,2,5,5-tetramethylpyrrolidine-*N*-oxyl, or 3-carbamoyl-proxyl; RIF, radiation-induced fibrosarcoma; EPR, electron paramagnetic resonance; EPRI, EPR imaging; BSO, L-buthionine-*S,R*-sulfoximine; ARCON, accelerated radiosensitization by carbogen and nicotinamide.

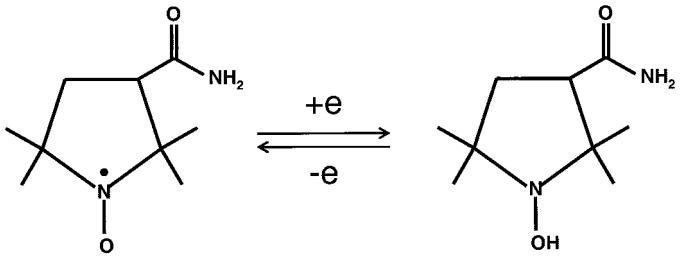

Fig. 1. Structure of 3-CP and its tissue metabolite. The "EPR active" 3-CP (3-carbamoyl-2,2,5,5-tetramethylpyrrolidine-*N*-oxyl, or 3-carbamoyl-proxyl) nitroxide probe undergoes one-electron reduction in tissues to "EPR-silent" hydroxylamine form.

Experiments were conducted according to the principles outlined in the Guide for the Care and Use of Laboratory Animals prepared by the Institute of Laboratory Animal Resources, National Research Council.

RIF-1 Tumor Growth. RIF-1 tumor cells were grown in monolayered culture until injection in mice. The mice were injected s.c. in their right hind leg with a single cell suspension of tumor cells (10^6 cells in 0.1 ml) in PBS. The animals were observed closely, and the tumors became palpable ~5 days after injection. Tumors were allowed to grow to a size of about 8–10 mm in the greatest dimension.

Tissue GSH Assay. Mice were injected (i.p.) with 2.25 mmol/kg (body-weight) of BSO in 100 μl of saline. Six h later, the animals were killed, and about 0.2–0.5 g of tumor tissue on the right leg and normal muscle tissue on the left leg were carefully excised and weighed. The tissues were placed in glass dounce homogenizer (5 ml) and homogenized with 1 ml of 200 mM methanesulfonic acid containing 5 mM diethylenetriaminepentaacetic acid (DTPA; pH <2.0). This homogenate was centrifuged for 30 min at 14,000 rpm at 4°C. The resultant supernatant was diluted 1:1 with mobile phase and stored frozen at −70°C for GSH assay.

The GSH assays were performed by high-performance liquid chromatography-electrochemical method (20). Samples were separated on a Polaris 5 μm, 0.4 × 20 cm C-18 column eluted with a mobile phase of 50 mM NaH_2PO_4, 0.05 mM octanesulfonic acid, and 2% acetonitrile adjusted to pH 2.7 with phosphoric acid and a flow rate of 1 ml/min. An ESA CoulArray detector was used with the guard cell set at +950 mV, electrode 1 at +400 mV, and electrode 2 at +880 mV. Full-scale output was set at 100 μA and peak areas were analyzed using the CoulArray software (ESA, Chelmsford, MA). A standard curve was obtained using a 10 μM-to-1 mM solution of GSH, from which concentrations of GSH were determined. The GSH values were expressed as μmol/g of tissue wet weight.

EPRI Instrumentation. Imaging measurements were performed using the EPRI instrumentation consisting of an L-band EPR spectrometer, three sets of water-cooled gradient coils and a personal computer-based data acquisition system (18, 21, 22). EPR spectra were recorded using a custom-built surface resonator (18, 23). The resonator consisted of two concentric quartz tubes, 10 and 12 mm in diameter, with the outer surfaces covered with silver foil strips forming a bridged loop-gap structure. The resonator structure was housed inside a metallic tubular shield with one open end, 10 mm diameter, functioning as the active surface. The resonator was capable of sampling a cylindrical volume measuring 10 mm in diameter and 5 mm deep. The open structure of this resonator was ideal for localized measurements on large objects and thus was not limited by the size of the object.

Animal Preparation. Mice were anesthetized by breathing air containing 1% isoflurane delivered through a nose cone. The tail vein was cannulated with a heparin-filled 30-gauge catheter for infusion of the nitroxide probes. Either the tumor in the right leg or the normal tissue (muscle) on the left leg was prepared for measurements. The hair on the observation spot of the skin was shaved and the animal was placed on a bedplate with a circular slot (20 mm diameter) in such a way that the observation spot was centered at the slot. The animal was secured to the plate with adhesive tape and placed on top of the resonator such that the tumor or the normal muscle was in direct contact with the active surface of the resonator. An IR lamp was used to maintain normal body temperature, which was measured using a rectal thermistor probe.

Projection Acquisition and Image Reconstruction. Projection data were acquired using angular sampling method. The projections were acquired as single scans (1024 points/projection) using constant sweep time. The measured projections were corrected for removal of hyperfine-based artifacts and deconvoluted with the corresponding zero-gradient projection (24). The deconvoluted projections were then convoluted with a Shepp-Logan filter and subsampled to 128 points for backprojection. A single-stage, filtered backprojection reconstruction algorithm was used to recover the image. Projection data acquisition and subsequent image reconstruction were performed using an Intel Pentium 600 MHz Personal Computer equipped with an IEEE-488 GPIB board (Capital Equipment Corporation, Burlington, MA).

Statistical Analysis. All of the data were expressed as mean ± SE. Comparisons among groups were performed by student's *t* test or one-way ANOVA, with Student-Newman-Keuls tests. The significance level was defined as $P < 0.05$.

RESULTS

Pharmacokinetics of nitroxide uptake and clearance from normal and tumor tissues of RIF-1 tumor-bearing mice were measured *in vivo* using EPR spectroscopy. 3-CP was used as a probe at a dose of 185 mg/kg. Mice were infused (bolus dose), *via* tail vein catheter, with a saline solution of 3-CP, and EPR spectra were measured continuously from the tumor on right leg or normal muscle tissue on the left leg. A few spectra, representative of the time course measurements from a RIF-1 tumor, are shown in Fig. 2. The field-swept EPR spectra are characterized by a triplet, arising because of hyperfine splitting from the ^{14}N nucleus, with coupling constants 15.78 G and 16.30 G. The unequal coupling constants, which are usually observed at low-frequency measurements, are caused by breakdown of the high-field

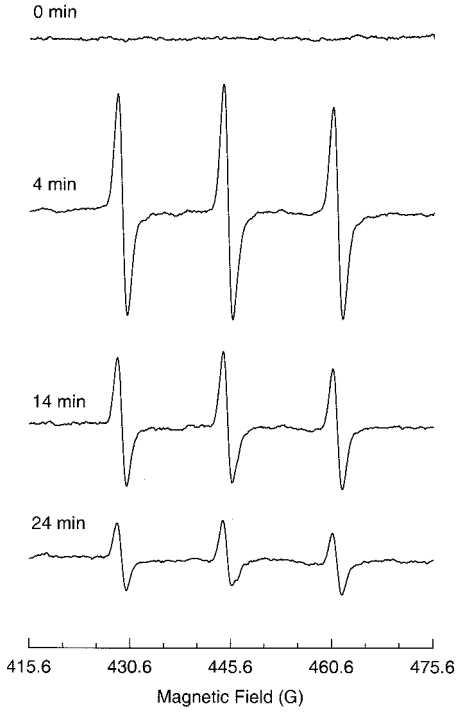

Fig. 2. EPR spectra of 3-CP nitroxide in a RIF-1 tumor. A tumor-bearing mouse under anesthesia was infused (i.v.) with a saline solution of 3-CP (185 mg/kg). The uptake and removal of the nitroxide in the tumor tissue was continuously measured *in vivo* using L-band (1.3 GHz) EPR spectrometer. The triplet signal attributable to 3-CP peaked at ~4 min and decayed gradually with a half-life of ~10 min. The triplet, arising because of hyperfine splitting from the ^{14}N nucleus, is characterized with coupling constants 15.78 G and 16.30 G and peak-to-peak width 1.50 G. Measurement parameters: microwave power 8 mW; modulation amplitude, 1.0 G; modulation frequency, 100 kHz; scan time, 15 s.

approximation, known as the "Breit-Rabi" effect. Each triplet of the spectrum is also characterized by a unique peak-to-peak width and amplitude. Whereas the coupling constant and width of the spectra remain more or less constant, the amplitude varies with time, reflecting changes in the nitroxide concentration in the tissue. Thus, either the area under the peak, measured as double integral of the spectrum, or peak-to-peak amplitude can be used as a quantitative measure of the nitroxide concentration, in arbitrary units. Fig. 3 shows a semilogarithmic plot of time course of the signal intensity of 3-CP in the normal and tumor tissues. The plot shows the data measured after the nitroxide intensity peaked, usually in about 3–4 min. It is observed that the nitroxide concentrations (in logarithmic units) in the tumor as well as normal tissues decrease linearly with time, suggesting that the clearance pharmacokinetics can be modeled by a pseudo-first order rate equation. The solid lines through the data points are linear fit to the respective data set suggesting compliance with a pseudo first-order rate law. The bar graph in Fig. 3*B* shows the measured pseudo first-order rate constants of nitroxide clearance in the tissues. The data represent mean ± SE of measurements on 3–5 mice per group.

To investigate the effect of GSH depletion on the rate of clearance of tissue nitroxide, the above pharmacokinetics experiments were also performed on tumor-bearing animals treated with BSO. Mice were injected (i.p.) with 2.25 mmol/kg BSO in saline, and the EPR measurements were made 6 h later. The dose and duration of BSO treatment were chosen to produce ~40–50% of GSH depletion from RIF tumors (4).

The nitroxide pharmacokinetic data indicate the following: (*a*) the nitroxide is reduced more rapidly in the tumor tissue compared with normal muscle tissue in the tumor-bearing mice; (*b*) the nitroxide reduction rate constant in the tumor of BSO-treated mice is decreased; and (*c*) the nitroxide reduction rate constant in the normal muscle tissue of BSO-treated tumor-bearing mice is not significantly different from that of untreated mice (data not shown). Taken together, the results suggest that BSO treatment provides a differential clearance of nitroxide in tumor tissues.

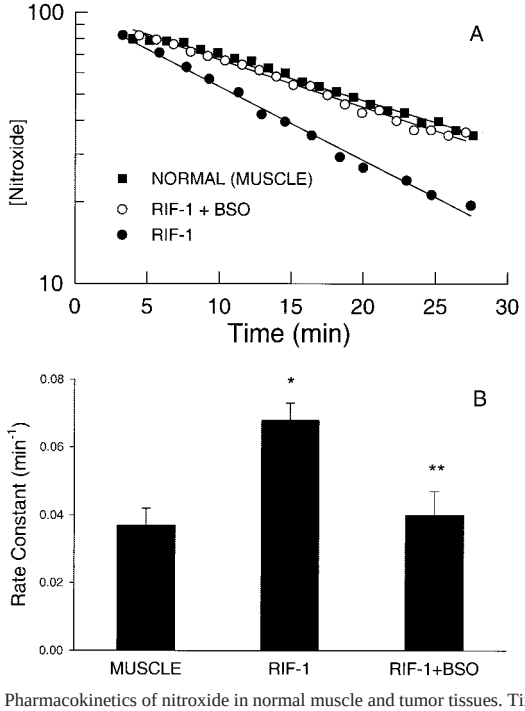

Fig. 3. Pharmacokinetics of nitroxide in normal muscle and tumor tissues. Time course of the EPR signal intensity of 3-CP in the normal leg muscle and tumor tissue of RIF-1 tumor-bearing mice, infused (i.v.) with a saline solution of 3-CP, were obtained by double integration of the spectra. *A*, The semilog plot shows the clearance of the nitroxide (in arbitrary units) as a function of time in the normal muscle (■) and tumor tissue (●) of untreated tumor-bearing mice and in the tumor tissue (○) of mice treated (i.p.) with BSO (2.25 mmol/kg) 6 h before the measurements. *The solid lines through the data points* are linear fit to the respective data set, which suggests compliance with a pseudo first-order rate law. *B*, bar-graph showing the measured pseudo first-order rate constants of nitroxide reduction in the tissues. The data represent mean ± SE of measurements on three to five mice per group. The rate constants were: untreated normal muscle, 0.037 ± 0.005 min^{-1}; untreated tumor, 0.063 ± 0.008 min^{-1}, and BSO-treated tumor, 0.052 ± 0.006 min^{-1}. *, significantly different from normal muscle; **, significantly different from untreated RIF-1 tissue.

The pharmacokinetic data presented above represents global measurements, *i.e.*, the data provide only an intensity-weighted mean clearance of the probe in the tissues. Spatially resolved changes in nitroxide intensity within the tumor volume are not obtained from the spectroscopic measurements. Because tumor tissues are characterized by significant heterogeneities in terms of redox status and oxygenation, it is desirable to obtain spatially resolved images of nitroxide distribution and clearance simultaneously within the tumor volume. This can be obtained using EPRI techniques that we have developed and used previously (18). Fig. 4 shows a few selected images from a series of two-dimensional spatial maps of nitroxide content in normal and BSO-treated tumor tissues obtained as a function of time after 3-CP infusion. It should be noted that these images were collected simultaneously on the same animals used for the measurement of pharmacokinetic data shown in Fig. 3. The data acquisition software was programmed to collect a series of alternating pharmacokinetic spectral (5 s) and image (~90 s) data on the same tissue for up to 30 min, immediately after infusion of the probe. Each time course image within the series, as shown in Fig. 4, was normalized with respect to the maximum intensity obtained within that series, usually in the images collected in about 4–6 min after infusion. The nitroxide reduction in the tumor of BSO-treated animals was slower than that in the tumor of untreated mice.

The images in Fig. 4 are 64 × 64 pixel images cropped from 128 × 128 pixels of original data obtained from a field of view of 20 × 20 mm^2. Thus, each pixel in the image represents a theoretical volume of 0.2 × 0.2 × 5.0 mm^3, although the actual resolution based on the number of projections and gradient field may limit the plane resolution to 1 mm and hence the volume to 1 × 1 × 5 mm^3. The series of image data can be used to follow time-dependent changes in each voxel within the image to obtain spatially resolved decay curves and hence rate constants. The rate constants for the clearance of the probe in each pixel were computed and displayed in the form of a color-coded image in Fig. 5. A frequency plot of the rate constants is also shown for each tissue in Fig. 5. The rate constant map and the frequency plot show the presence of a range of rate constants, which is a measure of heterogeneity in the redox status within each tissue.

The redox data show that the BSO treatment significantly decreases the rate constant of nitroxide reduction in the tumor tissue. It is known that BSO inhibits the γ-glutamylcysteine synthetase enzyme that is responsible for GSH synthesis (25). Studies have shown that tumor tissue levels of GSH can be depleted to very low levels without any toxicity (4). The effect of BSO treatment on the redox constants obtained in the present experiments, thus, can be attributed to alterations in the tissue GSH levels. To investigate the correlation between the observed rate constants and tissue GSH, the tissue levels of GSH were measured in the tissues of normal (control) and BSO-treated (same dose as for the EPR measurements) mice. The GSH assay data are shown in Fig. 6. The BSO-treated tissue data show a significant reduction in the GSH levels in the tumor tissue compared with untreated control. On the other hand, no significant differences were observed between treated and untreated normal tissues. The estimated GSH level (Fig. 6) correlates well with the nitroxide reduction rate constants (Fig. 3) in different tissues. Thus, it is evident that BSO causes a differential depletion among normal and tumor tissues.

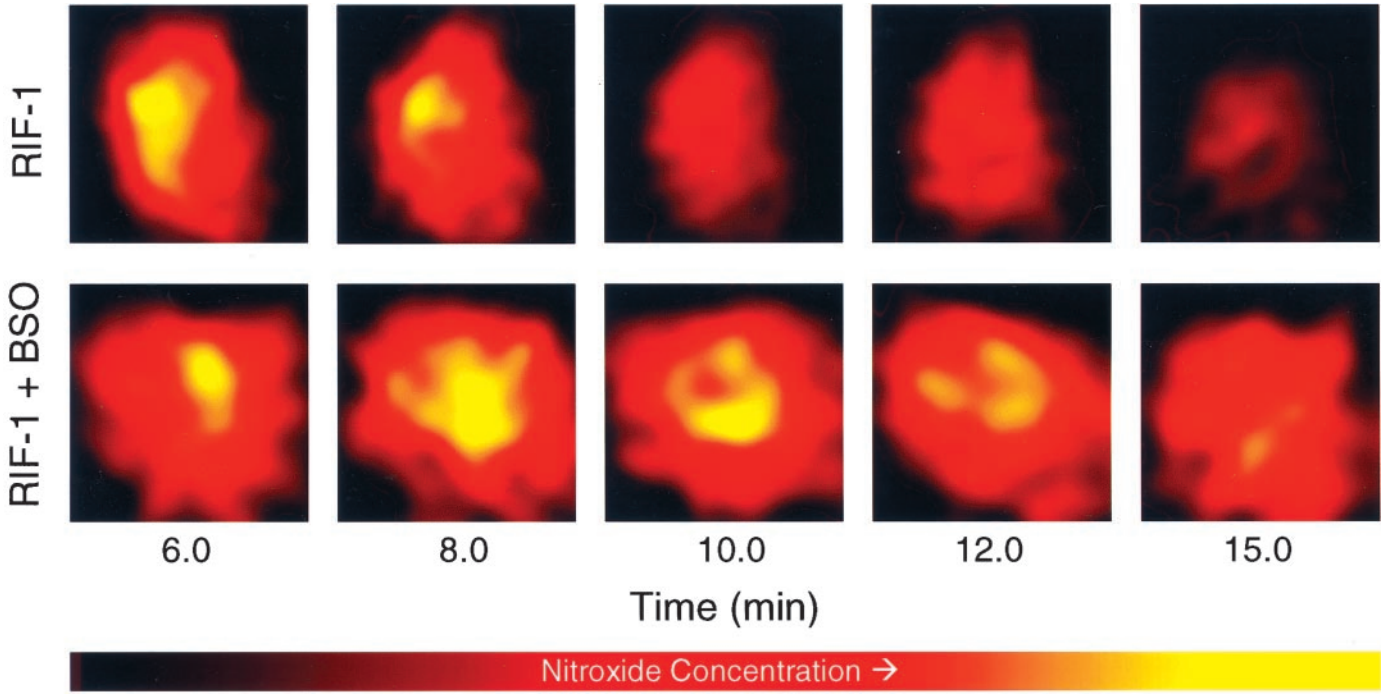

Fig. 4. Spatially resolved clearance of nitroxide in RIF-1 tumor tissue. After tail vein infusion of 3-CP, a series of two-dimensional images of the nitroxide from tumor (untreated and BSO-treated) were measured using L-band EPRI method. A few selected images and the corresponding approximate time after infusion are shown. The images represent the mean nitroxide concentration in a two-dimensional projection of the tissue volume (10×10 mm^2; depth, 5 mm) averaged over 1.5–2.0 min. The image data were acquired using a magnetic field gradient of 15 G/cm at 16 orientations in the two-dimensional plane. Each image within a series was normalized with respect to the maximum intensity in that series. The nitroxide in the tumor of BSO-treated mouse persisted longer, compared with that in the untreated mouse.

DISCUSSION

The treatment of malignant tumors by nonsurgical modalities like radiation or chemotherapy may be influenced both by the genetic properties of the tumor cells and the epigenetic factors of the tumor micromilieu (26, 27). While extensive research is presently ongoing to develop gene therapy strategies targeted to tumor cells, the development of therapeutic regimens to exploit the physiological differences between normal and malignant tissue may also provide options for improved treatment. Some of the physiological differences between normal tissue and tumors include oxygen status, redox status, and

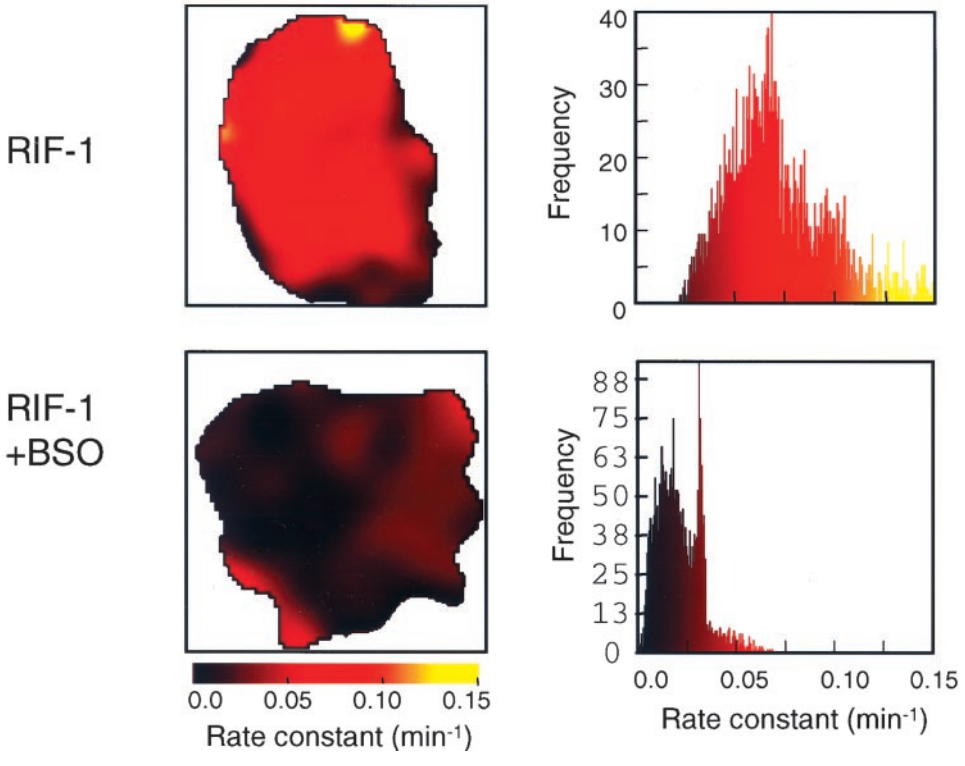

Fig. 5. Redox mapping of tumor. Two-dimensional spatial mapping of pseudo-first order rate constants (*left panels*) and frequency plot (*right panels*) of the nitroxide reduction rate constants in the RIF-1 tumors of untreated and BSO-treated mice were obtained from the time-course image data shown in Fig. 4.

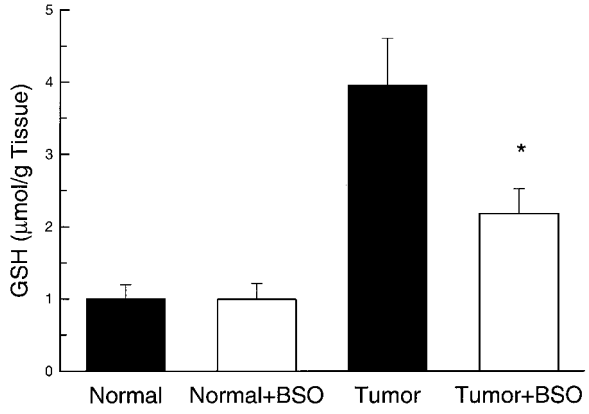

Fig. 6. GSH levels in normal muscle and RIF-1 tumors of untreated and BSO-treated mice. The normal muscle tissue and tumor tissue levels of GSH were measured in untreated RIF-1 tumor-bearing mice ($n = 7$) and in mice 6-h after treatment with 2.25 mmol/kg BSO ($n = 7$). *, significantly different from the untreated group.

intracellular pH (28, 29). These differences, at least in part, can result from the physical architecture of the tumors with compromised blood supply (30). Methods that can detect subtle differences in the above physiological parameters would greatly aid in devising appropriate treatment strategies. Techniques that enable rapid and noninvasive measurements of these two parameters in individual patients, therefore, would extend our knowledge and clinical acumen.

The present data obtained using *in vivo* EPR techniques and a nitroxide spin probe in RIF-1 tumor implanted in a C3H mouse model shows the differential physiology between normal and tumor tissue. After infusion, the reduction of the nitroxide, 3-CP, is enhanced in tumors compared with the normal tissue. The *in vivo* stability of nitroxides depends primarily on the ease of the oxidation of the nitroxide to the oxoammonium cation (31) or the reduction to the hydroxylamine (32). Consistent with this hypothesis are observations that the *in vivo* stability of the nitroxides is inversely related to the ease of reduction of the nitroxide. Furthermore, *in vivo* reduction of nitroxides is dependent on the oxygen content as well as on the levels of endogenous reducing agents such as GSH. The enhanced reduction of the nitroxide in tumor compared with normal tissue, thus, may be attributable to lower oxygen concentration as well as to the significantly enhanced GSH levels in the tumor.

In the pharmacokinetic experiments, we have followed changes in the nitroxide signal intensity in the tumor *in vivo* as a function of the postinfusion period. The measured rate of decrease of nitroxide signal intensity at the tumor site may depend on the following dynamic processes: (*a*) infusion of the probe into the tumor; (*b*) changes in the probe concentration caused by bioreduction in the tumor tissue; and (*c*) elimination of the probe out of the tumor volume by blood flow. Thus, the decrease in the EPR signal intensity of the nitroxide cannot be attributed to bioreduction processes alone. However, it has been reported by Gallez *et al.* (33) that bioreduction at the local site is the major factor that contributes to the overall decrease. This is also evident from the present work because different rate constants of clearance are observed between the tumor tissue and muscle on the nontumor-bearing leg. If perfusion is the major contributor, then any local measurement should reflect on the systemic levels of the probe, and, thus, the rates constants would have been identical between the two tissues. Thus, the clearance rate constant observed by this localized measurement can be used as a parameter of tumor tissue redox status, which is correlated to the bioreduction of the probe.

Several studies have shown that tissue oxygenation is an important factor that will affect the tissue redox status and hence the reduction rate of the nitroxide. Particularly, tissue hypoxia, which is known to be present in tumors, has been shown to enhance the bioreduction of nitroxides (18). Although this is evident from the enhanced rate of reduction from the tumor as compared with muscle tissue, which is relatively well oxygenated, the involvement of other factors, such as altered redox state and pH, may also be important.

GSH plays a central role in the maintenance of enzyme sulfhydral groups in the proper redox state (34). Because of this, alterations of the GSH redox state can have profound effects on cellular metabolism. GSH is present in significantly large quantities inside cells and it is a versatile protector. Some of the protective roles of the GSH include radical scavenging, restoration of damaged molecules by hydrogen donation, reduction of peroxides, and maintenance of protein thiols in the reduced state. Of these roles, hydrogen atom donation to DNA radicals is probably the most important. Because competing reactions are very rapid, particularly with oxygen in well-oxygenated normal tissues, high concentrations of GSH are required for protection. Thus, moderate depletion of GSH in normal cells has no effect on the radiosensitivity; whereas under hypoxic conditions, such as those that occur in tumor tissues, GSH may play a dominant protective role (35–37). Conversely, the depletion of GSH in the hypoxic tumor tissue may have beneficial effects on the treatment of tumors (38). The safety and efficacy of BSO-based metabolic alteration in cancer treatment have been extensively studied (4, 38). The results show that considerable variations exist in the effectiveness of GSH depletion depending on the tumor model and origin. Nevertheless, the method has the potential to offer therapeutic enhancements in such cases in which it is effective and may augment other procedures such as ARCON for radio- or chemotherapy (39–43).

In conclusion, noninvasive measurements and mapping of tumor redox status in tumor-bearing mice were performed using low-frequency EPR spectroscopy/imaging techniques. Implanted RIF-1 tumor in the right leg was studied, and the normal tissue on the left leg was used as control. Nitroxide pharmacokinetics showed overall higher magnitude and significant heterogeneity of reducing equivalents in the tumor tissue compared with normal tissue. Mice treated with BSO, a GSH-depleting agent, showed differential reduction in the tissue GSH levels and reducing equivalents. This differential reduction of reducing equivalents between the normal and malignant tissue may be useful for selective tumor killing.

REFERENCES

1. Schafer, F. Q. and Buettner, G. R. Redox environment of the cell as viewed through the redox state of the glutathione disulfide/glutathione couple. Free Radic. Biol. Med. *30:* 1191–1212, 2001.
2. Mitchell, J. B., and Russo, A. The role of glutathione in radiation and drug induced cytotoxicity. Br. J. Cancer, *8* (Suppl.)*:* 96S–104S, 1987.
3. Stratford, I. J., Adams, G. E., Bremner, J. C., Cole, S., Edwards, H. S., Robertson, N., and Wood, P. J. Manipulation and exploitation of the tumour environment for therapeutic benefit. Int. J. Radiat. Biol., *65:* 85–94, 1994.
4. Yu, N. Y., and Brown, J. M. Depletion of glutathione *in vivo* as a method of improving the therapeutic ratio of misonidazole and SR 2508. Int. J. Radiat. Oncol. Biol. Phys., *10:* 1265–1269, 1984.
5. Brown, J. M. SR 4233 (tirapazamine): a new anticancer drug exploiting hypoxia in solid tumours. Br. J. Cancer, *67:* 1163–1170, 1993.
6. Berliner, L. J. (ed.), Spin Labeling: Theory and Applications, Vol. 1. New York: Academic Press, 1976.
7. Berliner, L. J. (ed.), Spin Labeling: Theory and Applications. New York: Academic Press, 1979.
8. Kocherginsky, N., and Swartz, H. M. (eds.), Nitroxide Spin Labels: Reactions in Biology and Chemistry. Boca Raton, FL: CRC Press, 1995.
9. Canney, P. A., and Dean, S. Transforming growth factor β: a promotor of late connective tissue injury following radiotherapy? Br. J. Radiol., *63:* 620–623, 1990.
10. Couet, W. R., Brasch, R. C., Sosnovsky, G., and Tozer, T. N. Factors affecting nitroxide reduction in ascorbate solution and tissue homogenates. Magn. Reson. Imaging, *3:* 83–88, 1985.
11. Swartz, H. M. Principles of the metabolism of nitroxides and their implications for spin trapping. Free Radic. Res. Commun., *9:* 399–405, 1990.

12. Ishida, S., Kumashiro, H., Tsuchihashi, N., Ogata, T., Ono, M., Kamada, H., and Yoshida, E. *In vivo* analysis of nitroxide radicals injected into small animals by L-BAND ESR technique. Phys. Med. Biol., *34:* 1317–1323, 1989.
13. Berliner, L. J., and Wan, X. M. *In vivo* pharmacokinetics by electron magnetic resonance spectroscopy. Magn. Reson. Med., *9:* 430–434, 1989.
14. Utsumi, H., Ichikawa, K., and Takeshita, K. *In vivo* ESR measurements of free radical reactions in living mice. Toxicol. Lett. (Amst.), *82–83:* 561–565, 1995.
15. Kuppusamy, P., Wang, P., Zweier, J. L., Krishna, M. C., Mitchell, J. B., Ma, L., Trimble, C. E., and Hsia, C. J. Electron paramagnetic resonance imaging of rat heart with nitroxide and polynitroxyl-albumin. Biochemistry, *35:* 7051–7057, 1996.
16. Halpern, H. J., Peric, M., Yu, C., Barth, E. D., Chandramouli, G. V., Makinen, M. W., and Rosen, G. M. *In vivo* spin-label murine pharmacodynamics using low-frequency electron paramagnetic resonance imaging. Biophys. J., *71:* 403–409, 1996.
17. Hahn, S. M., Sullivan, F. J., DeLuca, A. M., Krishna, C. M., Wersto, N., Venzon, D., Russo, A., and Mitchell, J. B. Evaluation of tempol radioprotection in a murine tumor model. Free Radic. Biol. Med., *22:* 1211–1216, 1997.
18. Kuppusamy, P., Afeworki, M., Shankar, R. A., Coffin, D., Krishna, M. C., Hahn, S. M., Mitchell, J. B., and Zweier, J. L. *In vivo* electron paramagnetic resonance imaging of tumor heterogeneity and oxygenation in a murine model. Cancer Res., *58:* 1562–1568, 1998.
19. Tomasi, A., Albano, E., Iannone, A. C., Swartz, H. M., and Vannini, V. Reduction mechanism of the spin probe Tempol in liver microsomes. *In:* O. Hayashi, E. Niki, M. Kondo, and A. Yoshikawa (eds.), Medical, Biomedical and Chemical Aspects of Free Radicals, pp. 821–829. Amsterdam: Elsevier, 1988.
20. Lakritz, J., Plopper, C. G., and Buckpitt, A. R. Validated high-performance liquid chromatography-electrochemical method for determination of glutathione and glutathione disulfide in small tissue samples. Anal. Biochem., *247:* 63–68, 1997.
21. Kuppusamy, P., Chzhan, M., Vij, K., Shteynbuk, M., Lefer, D. J., Giannella, E., and Zweier, J. L. Three-dimensional spectral-spatial EPR imaging of free radicals in the heart: a technique for imaging tissue metabolism and oxygenation. Proc. Natl. Acad. Sci. USA, *91:* 3388–3392, 1994.
22. Kuppusamy, P., Chzhan, M., and Zweier, J. L. Development and optimization of three-dimensional spatial EPR imaging for biological organs and tissues. J. Magn. Reson. B, *106:* 122–130, 1995.
23. Kuppusamy, P., Wang, P., Shankar, R. A., Ma, L., Trimble, C. E., Hsia, C. J., and Zweier, J. L. *In vivo* topical EPR spectroscopy and imaging of nitroxide free radicals and polynitroxyl-albumin. Magn. Reson. Med., *40:* 806–811, 1998.
24. Kuppusamy, P., and Zweier, J. L. A forward-subtraction procedure for removing hyperfine artifacts in electron paramagnetic resonance imaging. Magn. Reson. Med., *35:* 316–322, 1996.
25. Griffith, O. W. Mechanism of action, metabolism, and toxicity of buthionine sulfoximine and its higher homologs, potent inhibitors of glutathione synthesis. J. Biol. Chem., *257:* 13704–13712, 1982.
26. Sutherland, R. M. Cell and environment interactions in tumor microregions: the multicell spheroid model. Science (Wash. DC), *240:* 177–184, 1988.
27. Sklar, M. D. The ras oncogenes increase the intrinsic resistance of NIH 3T3 cells to ionizing radiation. Science (Wash. DC), *239:* 645–647, 1988.
28. Jain, R. K. Barriers to drug delivery in solid tumors. Sci. Am., *271:* 58–65, 1994.
29. Kimura, H., Braun, R. D., Ong, E. T., Hsu, R., Secomb, T. W., Papahadjopoulos, D., Hong, K., and Dewhirst, M. W. Fluctuations in red cell flux in tumor microvessels can lead to transient hypoxia and reoxygenation in tumor parenchyma. Cancer Res., *56:* 5522–5528, 1996.
30. Secomb, T. W., Hsu, R., Dewhirst, M. W., Klitzman, B., and Gross, J. F. Analysis of oxygen transport to tumor tissue by microvascular networks. Int. J. Radiat. Oncol. Biol. Phys., *25:* 481–489, 1993.
31. Krishna, M. C., Grahame, D. A., Samuni, A., Mitchell, J. B., and Russo, A. Oxoammonium cation intermediate in the nitroxide-catalyzed dismutation of superoxide. Proc. Natl. Acad. Sci. USA, *89:* 5537–5541, 1992.
32. Belkin, S., Mehlhorn, R. J., Hideg, K., Hankovsky, O., and Packer, L. Reduction and destruction rates of nitroxide spin probes. Arch. Biochem. Biophys., *256:* 232–243, 1987.
33. Gallez, B., Bacic, G., Goda, F., Jiang, J., O'Hara, J. A., Dunn, J. F., and Swartz, H. M. Use of nitroxides for assessing perfusion, oxygenation, and viability of tissues: *in vivo* EPR and MRI studies. Magn. Reson. Med., *35:* 97–106, 1996.
34. Biaglow, J. E., Varnes, M. E., Clark, E. P., and Epp, E. R. The role of thiols in cellular response to radiation and drugs. Radiat. Res., *95:* 437–455, 1983.
35. Mitchell, J. B., Russo, A., Biaglow, J. E., and McPherson, S. Cellular glutathione depletion by diethyl maleate or buthionine sulfoximine: no effect of glutathione depletion on the oxygen enhancement ratio. Radiat. Res., *96:* 422–428, 1983.
36. Clark, E. P., Epp, E. R., Morse-Gaudio, M., and Biaglow, J. E. The role of glutathione in the aerobic radioresponse. I. Sensitization and recovery in the absence of intracellular glutathione. Radiat. Res., *108:* 238–250, 1986.
37. Biaglow, J. E., Varnes, M. E., Tuttle, S. W., Oleinick, N. L., Glazier, K., Clark, E. P., Epp, E. R., and Dethlefsen, L. A. The effect of L-buthionine sulfoximine on the aerobic radiation response of A549 human lung carcinoma cells. Int. J. Radiat. Oncol. Biol. Phys., *12:* 1139–1142, 1986.
38. Meister, A. Glutathione deficiency produced by inhibition of its synthesis, and its reversal; applications in research and therapy. Pharmacol. Ther., *51:* 155–194, 1991.
39. O'Dwyer, P. J., Hamilton, T. C., LaCreta, F. P., Gallo, J. M., Kilpatrick, D., Halbherr, T., Brennan, J., Bookman, M. A., Hoffman, J., Young, R. C., Comis, R. L., and Ozols, R. F. Phase I trial of buthionine sulfoximine in combination with melphalan in patients with cancer. J. Clin. Oncol., *14:* 249–256, 1996.
40. Gallo, J. M., Brennan, J., Hamilton, T. C., Halbherr, T., Laub, P. B., Ozols, R. F., and O'Dwyer, P. J. Time-dependent pharmacodynamic models in cancer chemotherapy: population pharmacodynamic model for glutathione depletion following modulation by buthionine sulfoximine (BSO) in a Phase I trial of melphalan and BSO. Cancer Res., *55:* 4507–4511, 1995.
41. Bernier, J., Denekamp, J., Rojas, A., Minatel, E., Horiot, J., Hamers, H., Antognoni, P., Dahl, O., Richaud, P., van Glabbeke, M., and Pierart, M. ARCON: accelerated radiotherapy with carbogen and nicotinamide in head and neck squamous cell carcinomas. The experience of the Co-operative Group of Radiotherapy of the European Organization for Research and Treatment of Cancer (EORTC). Radiother. Oncol., *55:* 111–119, 2000.
42. Bernier, J., Denekamp, J., Rojas, A., Trovo, M., Horiot, J. C., Hamers, H., Antognoni, P., Dahl, O., Richaud, P., Kaanders, J., van Glabbeke, M., and Pierart, M. ARCON: accelerated radiotherapy with carbogen and nicotinamide in non small cell lung cancer: a Phase I/II study by the EORTC. Radiother. Oncol., *52:* 149–156, 1999.
43. Bailey, H. H., Ripple, G., Tutsch, K. D., Arzoomanian, R. Z., Alberti, D., Feierabend, C., Mahvi, D., Schink, J., Pomplun, M., Mulcahy, R. T., and Wilding, G. Phase I study of continuous-infusion L-*S*,*R*-buthionine sulfoximine with intravenous melphalan. J. Natl. Cancer Inst. (Bethesda), *89:* 1789–1796, 1997.